ELSEVIER

Fusion Engineering and Design 54 (2001) 117–134

Fusion Engineering and Design

www.elsevier.com/locate/fusengdes

# Simulation studies of plasma shape identification and control in Korea Superconducting Tokamak Advanced Research

Hogun Jhang [a,*], C.E. Kessel [b], N. Pomphrey [b], Jin-Yong Kim [a], S.C. Jardin [b], G.S. Lee [a]

[a] *Korea Basic Science Institute, 52, Yeoeun-dong, Yusung-Ku, Taejon, South Korea*
[b] *Princeton Plasma Physics Laboratory, Princeton, NJ 08543, USA*

Received 24 February 2000; accepted 19 May 2000

**Abstract**

Simulation studies of plasma shape identification and shape control for the proposed Korea superconducting tokamak advanced research (KSTAR) are described. It is shown that the total number of magnetic measurements can be effectively reduced by considering the patterns of magnetic flux and fields, generated by plasma, along a prescribed measurement contour. The effect of eddy currents on shape identification is investigated in dynamic simulations. The isoflux control scheme and a standard PID control law are adopted for the development of a model shape control system. It is shown that appropriate weighting factors of poloidal field coils, incorporating the efficacy of each coil to a shape control point, can significantly reduce the total feedback power required for a shape control action. Finally, a shape control simulation using calculated flux errors, which correspond to a more realistic experimental situation, is presented. 

*Keywords:* Plasma; Tokamak; Magnetic flux

## 1. Introduction

For a successful operation of next generation tokamaks, such as international thermonuclear experimental reactor (ITER) or Korea superconducting tokamak advanced research (KSTAR)[1], it is essential to develop a reliable and powerful plasma control system. In the present paper, we report, as an effort to develop such a plasma control system in KSTAR, the simulation studies of a plasma shape control in the proposed KSTAR device. The analysis of fast time scale plasma position control system in KSTAR has been reported in [2]. A shape control system is a typical example of multi-input multi-output (MIMO) control system. It can be decomposed into three major components — magnetic measurements, the interpretation of the magnetic

* Corresponding author. Tel.: +82-42-8653607; fax: +82-42-8653619.
*E-mail address:* hgjhang@kstar.kbsi.re.kr (H. Jhang).

0920-3796/01/$ - see front matter 
PII: S0920-3796(00)00431-2

measurements (or the evaluation of shape errors), and the calculation of a series of feedback commands to actuate power supplies of poloidal field (PF) coils.

The typical magnetic measurements consist of magnetic flux loops and field probes placed along plasma facing components (PFCs) inside a tokamak vacuum vessel. Both the number and the location of magnetic measurements are important to obtain accurate shape information. Often, they have been determined empirically based on experiences. Here, we propose a simple method of finding crucial locations of magnetic measurements utilizing the patterns of magnetic flux and fields, generated by plasma, along a *measurement contour*. Here, the *measurement contour* is defined as a contour along which the magnetic measurements are to be placed. We found that the method made it possible to effectively reduce the total number of magnetic measurements.

Table 1
The nominal plasma parameters of the Korea superconducting tokamak advanced research (KSTAR) tokamak

| | |
|---|---|
| Plasma current, $I_p$ (MA) | 2 |
| Major radius, $R_0$ (m) | 1.8 |
| Minor radius, $a$ (m) | 0.5 |
| Elongation ($k_x$) | 2.0 |
| Triangularity ($\delta_x$) | 0.8 |
| Toroidal field, $B_0$ (T) | 3.5 |
| Reference configuration | Double null |

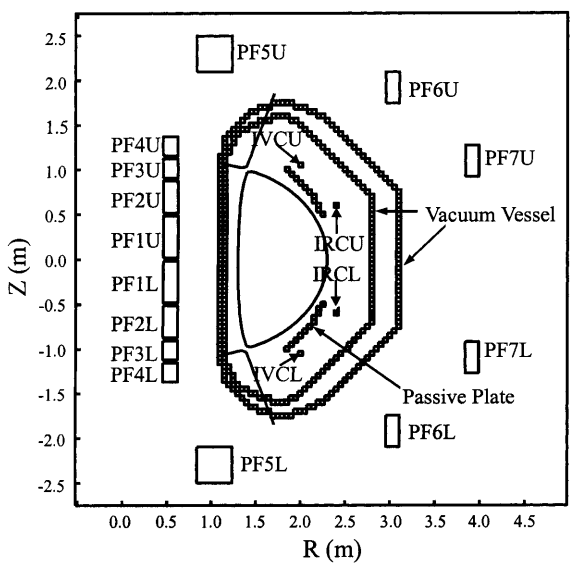


Fig. 1. Axisymmetric structure model of KSTAR used in TSC simulations. The passive structures include double-walled vacuum vessel and the passive plates, which are up–down symmetric and connected into saddle configuration. Two sets of internal control coils are denoted by IVC (2.00, $\pm 1.05$) and IRC (2.40, $\pm 0.60$), respectively.

The on-line evaluation of shape errors is crucial for a real-time shape control system because the shape errors can not be determined directly from magnetic measurements. A variety of methods possessing real-time computational capability have been proposed for the purpose of shape identification [3–11] and some of them are in current operation in the present-day tokamaks, such as JET [7], ASDEX-U [9], TCV [4], JT-60U [8] and DIII-D [11]. In the present work, we adopt the finite current element method [4], which is routinely used in TCV [12] experiments, to identify plasma shapes.

After shape errors are computed, feedback commands should be calculated to compensate them. In the present work, we adopt the *isoflux* method [11,13], in which some prescribed shape control points are forced to have the same flux value as a reference point. In order to economize a shape controller, it is necessary to minimize a total feedback power, yet yielding a good control performance. This can be achieved by properly incorporating the practical voltage limits of power supplies and the different capabilities of PF coils to control a specific shape control point. We will show that simple but appropriate weighting of PF coils reduces the total feedback power and current required for a shape control action.

Major plasma parameters of KSTAR are shown in Table 1 and an axisymmetric structure model of KSTAR being used in simulations (external PF coils, double-walled vacuum vessel, passive plate, and internal control coils) is shown in Fig. 1. The passive plate is 0.025-m thick, and comprises a pair of up–down symmetric plates electrically connected in a saddle configuration with a single toroidal break. The effective resistivity of KSTAR passive plate, calculated by SPARK code, has been found to be $4.36 \times 10^{-8}$ $\Omega$ m [2]. The double-walled vacuum vessel is made

of stainless steel (resistivity, $180.0 \times 10^{-8}$ Ω m) and assumed to be 0.02-m thick. As a simulation tool, we use tokamak simulation code (TSC) [14] throughout the paper.

The organization of present paper is as follows. In Section 2, plasma shape identification simulations are presented. First, the finite current element method for plasma shape identification is briefly described. Then, we identify some important locations of magnetic measurements based on the patterns of plasma-generated magnetic flux and fields along a measurement contour defined in KSTAR geometry. We construct reduced sets of which the total number of magnetic measurements is significantly reduced compared with that of original sets. The static and dynamic shape identification simulations are performed using the original and reduced magnetic diagnostic sets. The effect of eddy currents on plasma shape identification is addressed in dynamic simulations.

In Section 3, we discuss the problem of the control of a plasma shape in KSTAR. The efficacy of each PF coil on a particular shape control point is assessed and an appropriate weighting factor for each PF coil is evaluated. Then, the shape control simulations utilizing the evaluated PF coil weighting factors are performed and the results are compared with those obtained by using a standard constant PF coil weighting factor. Also, the shape control simulations using evaluated shape errors, which correspond to more realistic experimental situations, are performed. The impact of eddy currents on shape control performance is discussed.

Finally, a summary and some discussions are given in Section 4.

## 2. Plasma shape identification

### 2.1. Shape identification algorithm

As mentioned in Section 1, we employ the finite current element method [4] for the purpose of plasma shape identification. The current element method is used in TCV [12] experiments. In this approach, a plasma current is modeled by a set of grid of points inside the plasma. As shown in Fig. 2, we set up a rectangular grid of points inside the plasma and allow a pyramid-shaped current density to exist at each node by giving the bilinear basis function of the form [4],

$$F_j = \left\{1 - \frac{|R - R_j|}{\Delta R}\right\}\left\{1 - \frac{|Z - Z_j|}{\Delta Z}\right\},$$

where $R_j$ ($Z_j$) is the horizontal (vertical) coordinate of the $j$th node, and $\Delta R$ ($\Delta Z$) is the horizontal (vertical) width of a current element.

Each current element is defined by the current density at the node. The nodal current densities are determined by fitting the external magnetic measurements. We assume that the magnetic measurements consist of magnetic flux loops, field probes, and Rogowskii coils to measure the total plasma current and eddy currents in passive plates. It is also assumed that the measurements of PF coil currents are available as well as the magnetic measurements. Then, the nodal current densities are calculated by minimizing the cost function,

$$\varepsilon = \sum_{i=1}^{N_m}\left(\sum_{j=1}^{N_n} \bar{G}_{ij}(R_i, Z_i; R_j, Z_j)J_j - \psi_i^{\text{plasma}}\right)^2 + \alpha^2 \sum_{j=1}^{N_n} J_j^2 \quad (1)$$

Here, $N_m$ ($N_n$) is a total number of external measurements (current density nodes), $J_j$ is $j$th nodal current density, $\psi_i^{\text{plasma}} \equiv \psi_i^{\text{total}} - \psi_i^{\text{PF}} - \psi_i^{\text{eddy}}$, where $\psi_i^{\text{total}}$ is a measured value of flux (or fields), $\psi_i^{\text{PF}}$ is a flux value due to the external PF coils, and $\psi_i^{\text{eddy}}$ is the flux contribution from eddy currents at the $i$th measurement location, $\alpha$ is a small regularization parameter, and $\bar{G}_{ij}(R_i, Z_i; R_j, Z_j)$ is the average Green function between the $i$th measurement location and the $j$th node,

$$\bar{G}_{ij} = \int_{z_j-\Delta z}^{z_j+\Delta z}\int_{R_j-\Delta R}^{R_j+\Delta R} G_{ij}(R_i, Z_i; R_j, Z_j)\left\{1 - \frac{|R - R_j|}{\Delta R}\right\}\left\{1 - \frac{|Z - Z_j|}{\Delta Z}\right\}\mathrm{d}R\,\mathrm{d}Z.$$

Eq. (1) can be solved by the standard singular value decomposition analysis with a constraint on the total plasma current,

$$\int_S J(R, Z)\mathrm{d}R\,\mathrm{d}Z = I_{\text{p}},$$

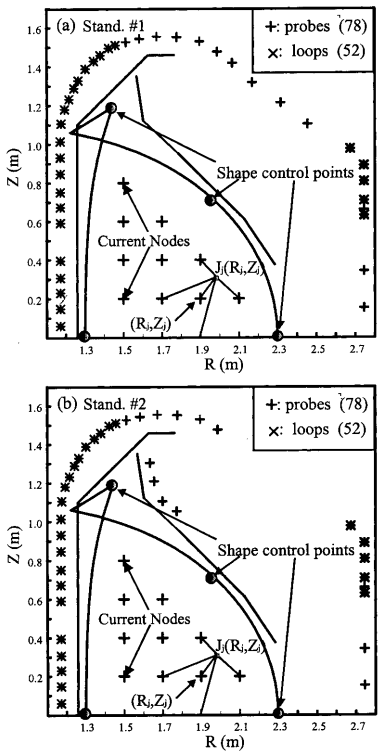


Fig. 2. The configurations of magnetic flux loops ( × ), and field probes ( + ) for the proposed magnetic diagnostic set # 1 (a) and # 2 (b). Also shown are the plasma current density nodes ( + , inside the plasma boundary) used in the simulations of plasma shape identification. All the magnetic measurements of set # 1 are located along the inside of inner vacuum vessel while four probes moved behind the outer divertor plate from the vacuum vessel for the set # 2. Fifty-two magnetic flux loops and 78 probes are used in both sets. We present only the upper portion of the magnetic measurements and the current density nodes for an up–down symmetric double null configuration. The bilinear basis function at the $j$th node to calculate a plasma current density is also shown.

where $I_p$ is the measured total plasma current, and $J(R, Z)$ is the calculated plasma current density at an arbitrary point inside the plasma,

$$J(R, Z) = J_j F_j.$$

It is remarked that the eddy currents in passive plates should be reconstructed if the measurement of eddy currents is not available.

We use 14 nodes for up–down symmetric plasmas while 24 nodes for up–down asymmetric ones. The number and the location of nodes are fixed in all the simulations presented in this paper. In fact, one of the advantages of the finite current element method compared with the filament method [3] is that the location of current density nodes do not have to be changed during an entire discharge, as discussed in [4].

After nodal current densities are computed, the fluxes at some points on PFCs and limiters are calculated. Then, the X-point, giving rise to $|\nabla\psi| = 0$, is searched in a specified divertor region and the flux at the X-point is computed using the calculated nodal current densities. From the calculated flux values at the limiter points and the X-point, we conclude whether plasma is limited or diverted and determine an edge flux, $\psi_{edge}$. A plasma boundary is determined by finding the points giving rise to $\psi = \psi_{edge}$.

### 2.2. Reduction of magnetic measurements

Both the number and the location of magnetic measurements are important to extract accurate shape information. In this subsection, we propose a possible method to identify some crucial measurement positions for the reconstruction of plasma shapes and apply it to KSTAR magnetic diagnostic in order to effectively reduce the total number of magnetic measurements.

Two magnetic diagnostic sets have been proposed in the design process of KSTAR and they are shown in Fig. 2. The set # 1 is composed of 52 flux loops and 78 ($B_t$, $B_n$) probe pairs located along a inner vacuum vessel, and the set # 2 is the same as the set # 1, except for the fact that four probe pairs have been moved behind outer divertor plates from the nearby vacuum vessel. The two configurations cover an entire space available where the magnetic measurements can be placed. Then, the optimization process can be regarded as eliminating some excess magnetic measurements starting from the proposed configurations.

A possible approach to determine crucial measurements is to exclude each measurement in turn and to perform many reconstruction simulations to rank the importance of each measurement. An obvious shortcoming of this trial-and-error type

approach is that it requires a time-consuming iteration procedure to rank each measurement according to its importance to the shape reconstruction. Furthermore, it will be difficult to reason out why some selected measurements are superior to the eliminated ones although we choose some crucial measurements from the iteration procedure.

Our approach is to trace the patterns of magnetic flux and fields, generated by plasma, along a measurement contour. Here, the *measurement contour* is defined as a contour along which the magnetic measurements are assumed to be placed. The basic idea is that the magnetic flux and field patterns, generated by a reconstructed plasma current distribution, along the measurement contour should follow the exact ones as closely as possible in order to obtain an accurate shape identification from the magnetic measurements. In this sense, the patterns of plasma-generated magnetic flux and fields along the measurement contour provide important information about which locations are important for a proper interpretation of magnetic diagnostic signals. We remark that this approach to determine important locations becomes more accurate as a measurement contour gets closer to a plasma boundary. In the present paper, the measurement contour is adjusted to the path along which the magnetic measurements of the set #1 are placed.

Fig. 3 shows the patterns of plasma-generated magnetic flux ($\psi^{\text{plasma}}$) and fields ($B_R^{\text{plasma}}$ and $B_Z^{\text{plasma}}$) along the measurement contour produced by standard low [$\beta = 0.2\%$ ($\beta_N = 0.3$), $l_i(3) = 1.0$, $I_p = 2.0$ MA, $\kappa = 2.0$, $\delta = 0.8$, $B_t = 3.5$ T] and high [$\beta = 4.0\%$ ($\beta_N = 3.5$), $l_i(3) = 0.8$, $I_p = 2.0$ MA, $\kappa = 2.0$, $\delta = 0.8$, $B_t = 3.5$ T] KSTAR plasmas. The poloidal angle ($X$-axis) in Fig. 3 is defined by, $\theta \equiv \int_0^P \mathrm{d}s / \oint \mathrm{d}s$, where $\int_0^P \mathrm{d}s$ is the poloidal path length of a point $P$ in the measurement contour, and $\oint \mathrm{d}s$ is the total poloidal path length of the measurement contour. It is obvious from Fig. 3 that both the plasmas exhibit similar patterns.

The most relevant locations of magnetic measurements can be found by the consideration of Fig. 3. The horizontal magnetic field ($B_R^{\text{plasma}}$) and the poloidal flux ($\psi^{\text{plasma}}$) show nonlinear wiggly structures while the vertical magnetic field ($B_Z^{\text{plasma}}$) represents nearly linear dependence. The approximately linear dependence of $B_Z^{\text{plasma}}$ along the measurement contour implies that the variation in $B_Z^{\text{plasma}}$ is unimportant to choose important measurement locations. It is sufficient to place the probes along the measurement contour with approximately equal spacing to follow the exact pattern of $B_Z^{\text{plasma}}$. However, the reconstructed patterns of $B_R^{\text{plasma}}$ and $\psi^{\text{plasma}}$ will fail to follow the exact ones if we place the measurements in equal spacing, which will eventually result in the errors in a shape identification process. Thus, the important measurement locations should be determined by following the patterns of $B_R^{\text{plasma}}$ and,$\psi^{\text{plasma}}$ emphasizing the position around the local minimum and/or maximum values of $\psi^{\text{plasma}}$ and $B_R^{\text{plasma}}$. It is evident from Fig. 3 that the most important measurement locations lies in the range $100 \leq \theta \leq 140°$, which corresponds to the region in the vicinity of X-point.

In order to effectively eliminate some excess magnetic measurements from the original set, we have established the following iteration process. First, we retain magnetic measurements located near humps in $\psi^{\text{plasma}}$ and $B_R^{\text{plasma}}$ patterns, especially in the range of $100 \leq \theta \leq 140°$. Second, we eliminate as many measurements as possible in the linear region of the flux and field patterns, yet following exact patterns of $\psi^{\text{plasma}}$ and $B_R^{\text{plasma}}$. Third, we perform shape identification simulations using both the reduced and the original set, and compare the results. If the two results are not comparable, we return to the second stage and put some more measurements. The process is iterated until the two results are almost identical. Usually, only two or three more iterations are required to obtain an effectively reduced set.

In this way, we determined two reduced magnetic diagnostic sets (RS1 and RS2) corresponding to the two original sets (#1 and #2). Fig. 4 shows the reduced sets, which are composed of 28 loops and 40 probes. The shape identification accuracy utilizing the reduced sets is comparable to that using the original sets, as will be shown in the subsequent subsection.

### 2.3. Simulations of plasma shape identification

#### 2.3.1. Static simulations

After determining a shape identification algorithm and magnetic diagnostic sets, we perform static simulations for the reference plasma equilibria in KSTAR. Here, we consider three representative equilibria for KSTAR plasmas; high $\beta[\beta_N = 3.5,\ l_i(3) = 0.8]$, low $\beta[\beta_N = 0.3,\ l_i(3) = 1.0]$, and a reversed shear plasma. As usual, numerically calculated values of magnetic flux and fields at each measurement location are used to simulate the measurement data. A maximum random measurement error, originating from a measurement process, is fixed to be 2% for magnetic flux and field measurements and 1% for a plasma current measurement,

$$\psi_i = \psi_{i\mathrm{E}}(1 + 0.02r), \quad B_i = B_{i\mathrm{E}}(1 + 0.02r),$$
$$I_\mathrm{p} = I_{\mathrm{pE}}(1 + 0.01r),$$

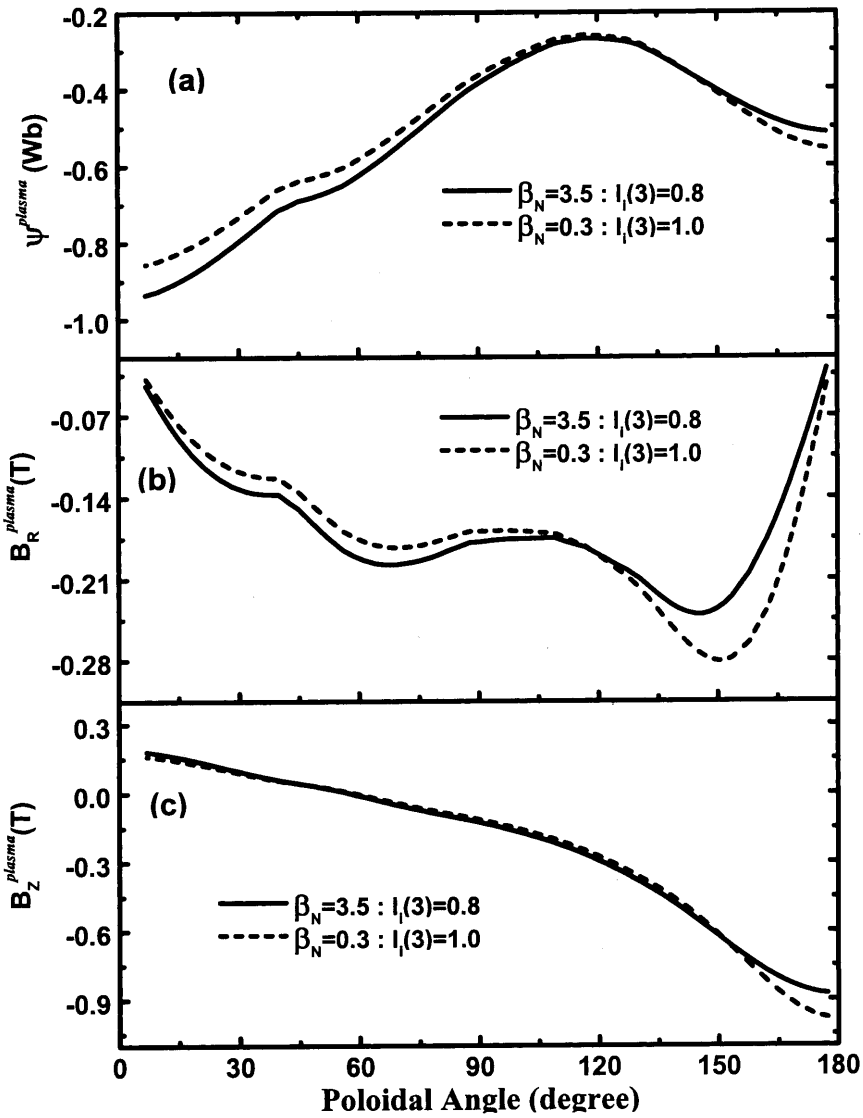


Fig. 3. Poloidal variation of plasma-generated (a) magnetic flux ($\psi^{\mathrm{plasma}}$); (b) radial ($B_R^{\mathrm{plasma}}$), and (c) vertical ($B_Z^{\mathrm{plasma}}$) magnetic fields for standard low [$\beta_N = 0.03$, $l_i(3) = 1.0$] and high [$\beta_N = 3.5$, $l_i(3) = 0.8$] beta equilibria in KSTAR. Here, the poloidal angle is defined by the poloidal path length of a measurement position divided by a total poloidal path length of a measurement contour.

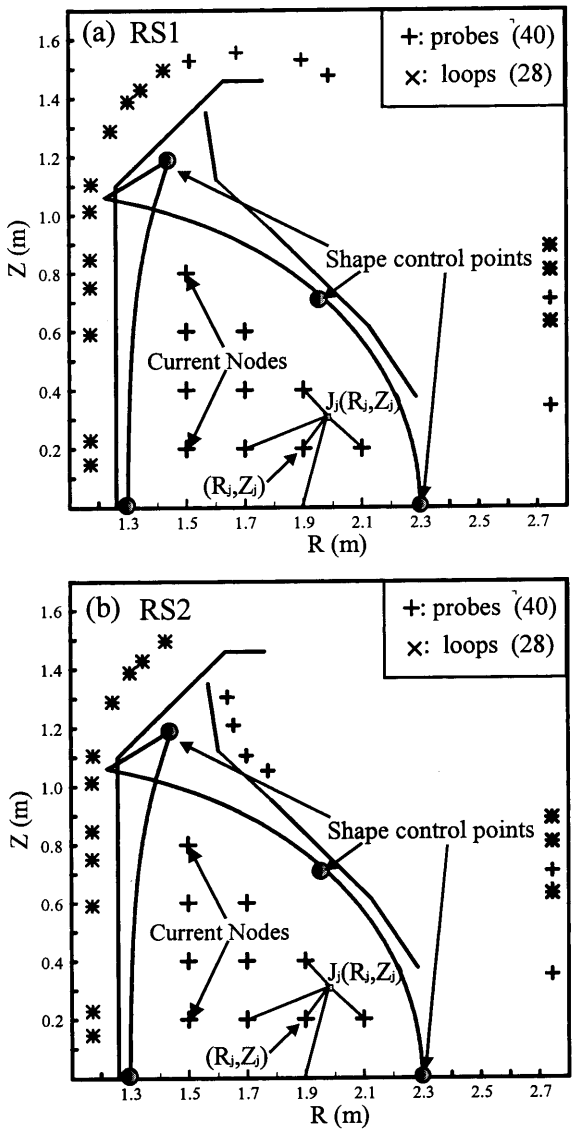


Fig. 4. The configurations of reduced magnetic diagnostic sets, (a) RS1 and (b) RS2. The reduced sets are found by considering the patterns of magnetic flux and fields along a measurement contour. RS1 corresponds to set # 1 and RS2 to set # 2. Twenty-eight flux loops and 40 magnetic probes are used in both the sets.

where $\psi_i$ ($B_i$) is an actual value to be used in simulations, $\psi_{i\mathrm{E}}$ ($B_{i\mathrm{E}}$) is an exact numerical value at the $i$th flux (field) measurement position calculated by TSC, and $r$ is the uniform random number within $[-1, 1]$. In order to obtain a statistically reliable result, a shape reconstruction is repeated over 100 times using different random numbers.

Fig. 5 shows the poloidal variations of shape identification error for (a) a high $\beta$, (b) a low $\beta$ and (c) a reversed shear plasma using different magnetic diagnostic sets (# 1, # 2, RS1 and RS2). Here, the shape identification error, denoted by $\Delta$, is defined by,

$$\Delta = \sqrt{(R_{\mathrm{exact}} - R_{\mathrm{rcnt}})^2 + (Z_{\mathrm{exact}} - Z_{\mathrm{rcnt}})^2}$$
$$= \sqrt{(\Delta R)^2 + (\Delta Z)^2}$$

where $R_{\mathrm{exact}}$ ($Z_{\mathrm{exact}}$) is an exact value of the horizontal (vertical) position of a last closed flux surface calculated by TSC and $R_{\mathrm{rcnt}}$ ($Z_{\mathrm{rcnt}}$) is that obtained from the reconstruction of a plasma shape. A shape error shown in Fig. 5 represents

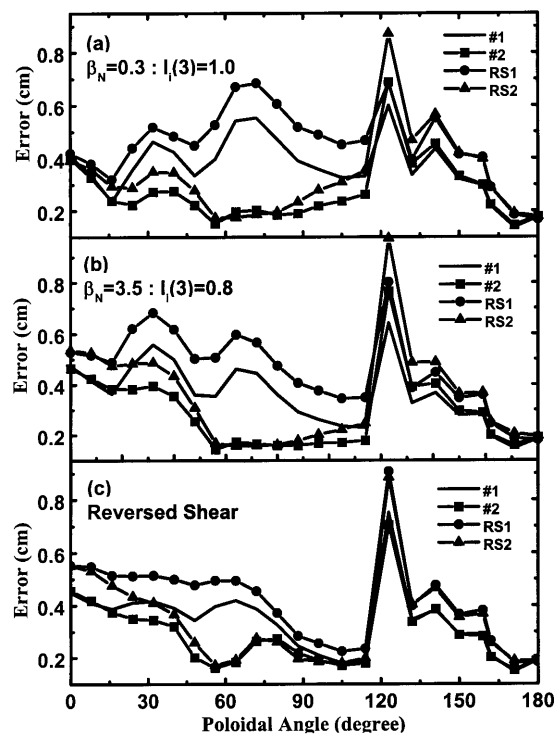


Fig. 5. Poloidal variation of an average error in shape identification for (a) low $\beta[\beta_N = 0.3,\ l_i(3) = 1.0]$ (b) high $\beta[\beta_N = 3.5,\ l_i(3) = 0.8]$ and (c) reversed shear plasmas in KSTAR. A 2% maximum random error for the measurements of magnetic flux and fields, and a maximum 1% error for the measurement of a plasma current have been included. A shape error is averaged over 100 different random simulations.

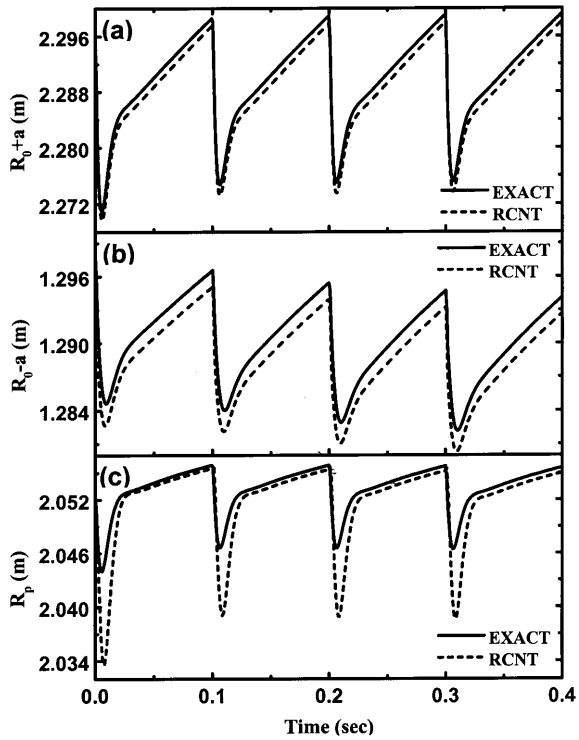


Fig. 6. Comparison between the reconstructed and the exact values of (a) $R_0 + a$; (b) $R_0 - a$, and (c) $R_p$, which is the $R$ coordinate of the nearest point to passive plate, in a dynamic shape identification simulation corresponding to a ELM-like oscillation.

an averaged value over 100 different random simulations.

It is manifested from Fig. 5 that the finite current element method provides an accurate determination of plasma shapes and is insensitive to the plasma parameters, such as $\beta$, $l_i$ and profile shape. The reduced sets, RS1 and RS2, show a similar degree of accuracy compared with that of original sets, $\#1$ and $\#2$, which confirms the effectiveness of the optimization method in the previous section. The four probe pairs behind the divertor plates turn out to be important to improve the shape identification accuracy on the outboard side, as is shown in Fig. 5.

### 2.3.2. Dynamic simulations

The dynamic plasma shape identification simulations are important to confirm that a proposed method can accurately predict the various shapes in real experiments. Another purpose of the dynamic simulations is to establish the importance of the measurement of eddy currents on shape identification. The finite current element algorithm can incorporate the effect of eddy currents if the eddy currents are directly measured. Neglecting the eddy currents will result in an error in diagnostic interpretation, leading to the miscalculation of a plasma shape.

In the present work, we perform dynamic simulations for two representative cases — a plasma in fast radial motion and a plasma undergoing fast vertical movement. It is remarked that each simulation presented in this subsection has been repeated using four different magnetic diagnostic sets ($\#1$, $\#2$, RS1 and RS2) although we will present only the results obtained by using set $\#1$. Also, we assume that the currents in PF and IC coils are known in the following simulations.

The first simulation is to reconstruct plasma shapes when a high $\beta$ plasma undergoes an edge localized mode (ELM)-like oscillation, which involves 20% $\beta$ drop every 100 ms in the recovery of its internal energy between the cycle. The radial control coil (IRC in Fig. 1) acts to restore the outermost flux surface ($R_0 + a$) to its original position. In this simulation, we assume that the measurement of eddy currents is not available. Fig. 6 shows the comparisons of the time histories of (a) the outermost flux surface ($R_0 + a$), (b) the innermost flux surface ($R - a$), and (c) the $R$ coordinate of the passive plate point ($R_p$), which is defined as the nearest plasma boundary point to the passive plate, between exact (calculated by TSC) values and reconstructed ones. Also, Fig. 7a and b show the comparisons of the time histories of $R$ and $Z$ coordinates of a X-point ($R_x$, $Z_x$), between the exact values and the reconstructed ones, and Fig. 7c represents a total up–down symmetric eddy current and the current in radial control coil (IRC) during the simulation. We can ascertain from Figs. 6 and 7, that the critical shape points are identified quite accurately. The passive plate point ($R_p$) gives rise to the maximum shape error of about 1 cm. A maximum up–down symmetric eddy current is found to be about 20 kA (1% of the total plasma current), as shown in

Fig. 7c. The total eddy current is not so large because the passive plates are electrically connected in a saddle configuration with a resistive connector to the vacuum vessel. A large gap resistance (total 300 or 600 μΩ for each plate) prevents the up–down symmetric current from flowing in each plate. We have observed that a up–down symmetric eddy current up to 20 kA, caused by either the radial displacement of a plasma column or the change in plasma current, does not affect the overall shape identification accuracy. The error in shape identification becomes large as a total eddy current exceeds 20 kA.

In order to investigate the effect of eddy currents, the previous simulation has been repeated on the assumption that the eddy currents in passive plates are measured. Fig. 8 shows the comparisons of the errors of (a) $R_0 + a$; (b) $R_0 - a$; (c) $R_p$, and (d) $R_x$, between with and without knowing the eddy currents in passive plates. Two general conclusions can be drawn from Fig. 8. First, the eddy current effect is transient on a shape control time scale. It depends primarily on the $L/R$ time of nearby conducting structures. The transient errors in shape identification, however, can lead to initial oscillations of PF coil currents and voltages when the shape identification process is combined into a shape controller, as will be shown in the next section. Second, the eddy current effect in shape identification is different from point to point. The error in $R_0 - a$ is maximum about 3 ms, which is the order of $L/R$ time of the vacuum vessel, while that of $R_p$ is maximized around 10 ms, which is the order of $L/R$ time of a passive plate with equivalent total resistance of 600 μΩ. A relatively large error in $R_p$ is originated from the larger eddy currents in the passive plate compared with the eddy currents in the vacuum vessel, and relatively small error in $R_0 + a$ is due to the large distance of $R_0 + a$ from nearby passive structures.

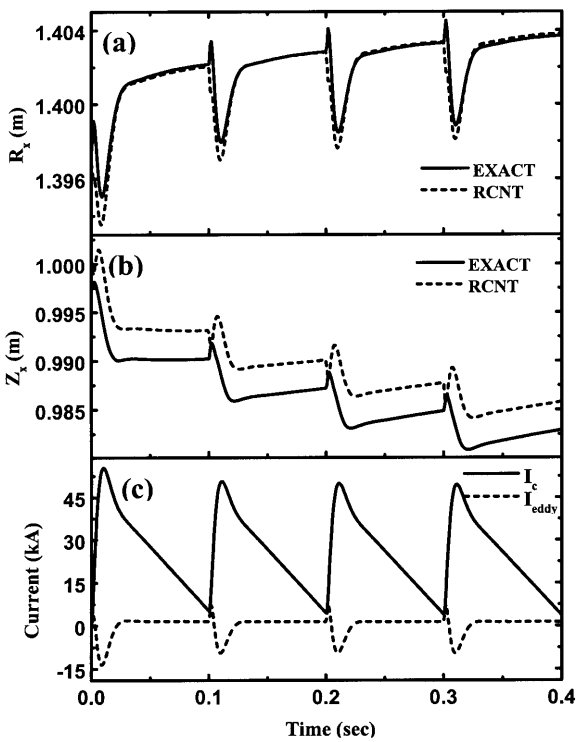


Fig. 7. (a) Comparison of the reconstructed and the exact values of $R$ coordinate, and (b) $Z$ coordinate of a X-point during the simulation in Fig. 6. Also shown are (c) the current in radial control coil (IRC), and a total up–down symmetric eddy current during the simulation.

In real experiments, the KSTAR plasma with a highly elongated shape is expected to undergo a high frequency vertical fluctuation. Because the PF coils in KSTAR are made of superconductors, they can not respond to such a fast time scale to stabilize the unstable vertical plasma motion. Thus, a plasma position control system should be decoupled from a shape control system. In such a case, the identification of a time averaged plasma shape would be meaningful for the purpose of a shape control. The second simulation is to reconstruct a *time averaged* plasma shape when a plasma undergoes a high frequency vertical fluctuation. We assume that the frequency bandwidth of all the relevant magnetic measurements (flux loops, field probes, and Rogowskii coils) is 10 kH$z$ and a shape reconstruction is performed every 10 ms. The time-averaged diagnostic data,

$$\bar{\psi}_i = \frac{1}{\Delta T}\int_{T_0}^{T_0+\Delta T}\left\{\frac{\psi_i^{\mathrm{up}}(t)+\psi_i^{\mathrm{down}}(t)}{2}\right\}\mathrm{d}t$$

$$\bar{I}_p = \frac{1}{\Delta T}\int_{T_0}^{T_0+\Delta T} I_p(t)\mathrm{d}t$$

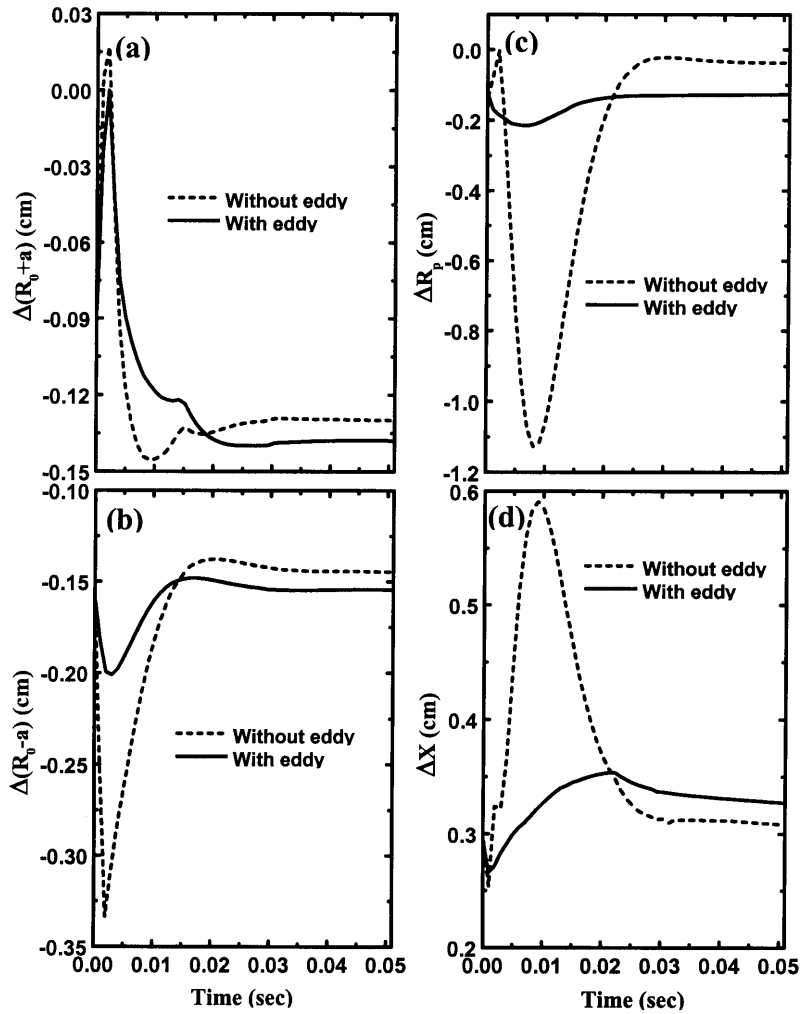


Fig. 8. Errors in shape identification with and without knowing eddy currents for the dynamic simulation in Figs. 6 and 7. The errors in (a) $R_0 + a$; (b) $R_0 - a$; (c) $R_p$, and (d) X-point are shown, respectively.

$$\bar{i}_c = \frac{1}{\Delta T}\int_{T_0}^{T_0+\Delta T} i_c(t)\mathrm{d}t$$

where $\Delta T$ is the duration of a shape reconstruction (10 ms), $\psi_i^{up}(t)$ ($\psi_i^{down}(t)$) is the $i$th magnetic flux or field measurement above (below) the mid-plane, $I_p(t)$ is a plasma current at time $t$, and $i_c(t)$ is time-varying coil currents (both PF and IC coils), are used for the purpose of a time-averaged shape identification. Note that we use up–down averaged flux and field measurements to cancel out the vertically fluctuating part of signals for an up–down symmetric double null configuration.

Fig. 9a and b show the time histories of magnetic axis and currents in vertical control coils (IVC), respectively, during the simulation. Fig. 10 represents a comparison between an exact plasma boundary at $t = 0$ and the reconstructed plasma boundaries at $t = 50$ and 100 ms. The reconstructed plasma boundaries are determined by finding 22 boundary points along a poloidal direction. The accuracy of time-averaged shape identification is excellent, as can be seen in Fig. 10. It is these reconstructed plasma shapes in Fig. 10 that one can expect to obtain in real experiments.

The up–down asymmetric eddy currents caused by a vertical plasma movement do not deteriorate the accuracy of the time-averaged plasma shape identification in so far as the vertical movement is small (nominal flat-top plasma free of disruptions).

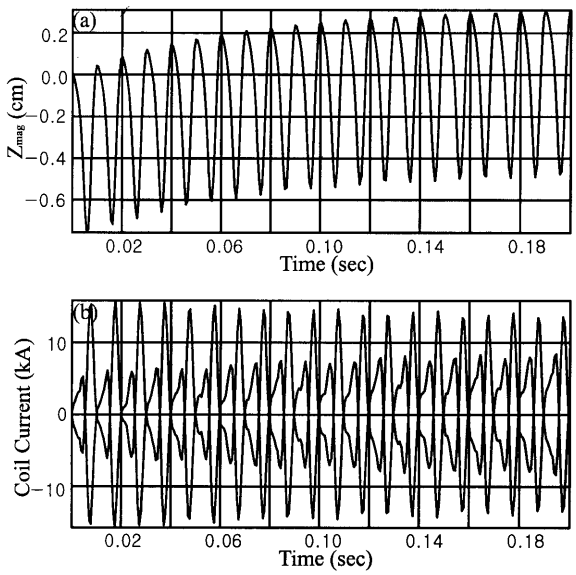


Fig. 9. Time histories of (a) magnetic axis ($Z_{mag}$), and (b) the currents in vertical control coil (IVC) for the simulation of time-averaged shape identification in a vertically fluctuating plasma.

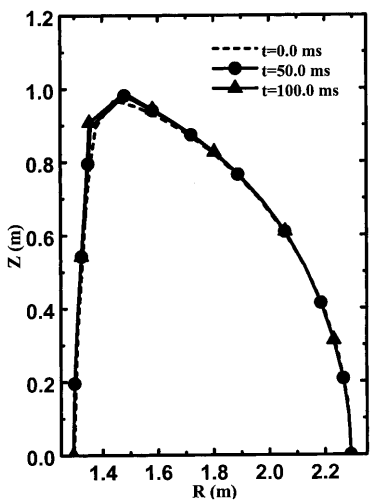


Fig. 10. Comparison of time-averaged shapes at $t = 50$ and 100 ms with an original shape at $t = 0$ ms. A plasma shape is identified every 10 ms using time-averaged measurement signals and coil currents. A reconstructed shape is determined by finding 22 points along a plasma boundary.

## 3. Shape control simulations

### 3.1. Shape control algorithm

A shape control system is a typical example of the multi-input multi-output (MIMO) control system which uses PF coil power supplies as actuators to correct shape errors. A shape control algorithm consists of the calculation of shape errors and the generation of a series of power supply commands to compensate the shape errors. A linear optimal controller algorithm has been applied to the design study of ITER shape control system [15,16], and a linear orthogonal shape control system, utilizing pre-calculated power supply commands giving rise to unit displacement of shape errors, has been adopted for Alcator C-Mod [17].

In the present work, we consider a standard PID feedback control system, and adopt the isoflux control scheme [11,13], which makes some prescribed shape control points have a same flux value with a reference point. In a nominal diverted plasma, the natural choice of a reference is an X-point. We choose four shape control points on a plasma boundary in a nominal state — the outermost flux surface ($R_0 + a$, 0), the innermost flux surface ($R_0 - a$, 0), the passive plate point ($R_p$, $Z_p$) and the outer strike point ($R_{st}$, $Z_{st}$). The plasma shape identification method described in the previous section is used to calculate flux errors. Here, a flux error is defined as a difference between the flux at the X-point and the flux value at a shape control point.

The generation of actuation signals is the core part of the design of a shape controller. The feedback currents are calculated by minimizing

$$\varepsilon = \sum_{i=1}^{N_p} \left( \sum_{j=1}^{N_c} G_{ij} \Delta I_j - \Delta \psi_i \right)^2 + \sum_{j=1}^{N_c} \alpha_j \Delta I_j^2, \qquad (2)$$

where $N_p$ ($N_c$) is the total number of critical shape control points (PF coils), $G_{ij}$ is the Green function relating the poloidal flux at the $i$th shape control point to the unit current at the $j$th PF coil, $\Delta I_j$ is the feedback current for the $j$th PF coil, $\Delta \psi_i$ is the

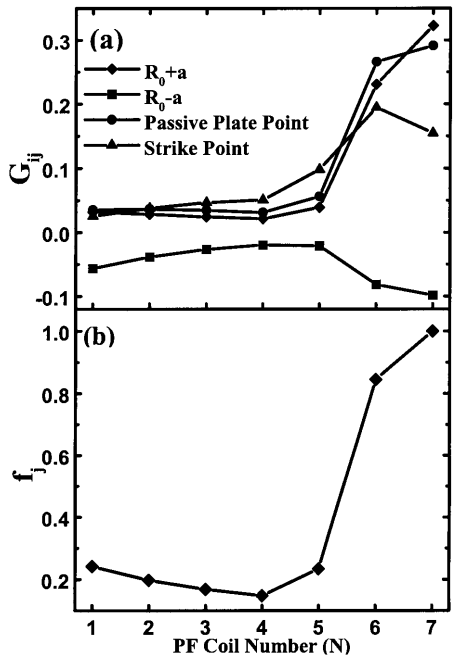


Fig. 11. (a) Green functions between four different shape control points and seven PF coils in KSTAR. (b) The average coil weighting factor, $\bar{f}_j$, in Eq. (3) is shown as a function of PF coil number. The PF coil numbering is identical to that of Fig. 1.

flux difference between a shape control point and a X-point, and $\alpha_j$ represents a weighting factor for the $j$th PF coil.

Each PF coil has a different influence on each shape control point. The Green function $G_{ij}$ reveals this different impact. Fig. 11a shows the Green function between the seven KSTAR PF coils and the four shape control points. It is obvious that PF6 and PF7 are the most effective because they are located on the outboard side. The calculation of feedback signals using Eq. (2) with constant $\alpha_j$ incorporates the efficacy of each PF coil to correct a flux error because it is based on the Green function formalism.

Practical power supplies, however, have their own voltage limits. The effectiveness of a shape control action would be degraded if a voltage of a power supply is saturated. For instance, PF6 and PF7 would reach their voltage limits quickly compared with other PF coils. For a more effective control action, it is required that the voltage saturation should be avoided or the duration of voltage saturation should be minimized. In order to avoid voltage saturation, we need a compensation factor and this can be achieved by systematically determining the $\alpha_j$ in Eq. (2). In order to determine $\alpha_j$, we define a normalized Green function,

$$\hat{G}_{ij} = \frac{G_{ij}}{G_{i7}}.$$

Then, an average influence factor is given by

$$\bar{f}_j = \sum_{i=1}^{N_p} \frac{\hat{G}_{ij}}{N_p} \tag{3}$$

The $\bar{f}_j$ is defined for each PF coil and Fig. 11b shows $\bar{f}_j$ as a function of PF coil number. Note that we do not use an absolute influence factor,

$$\bar{f}'_j = \frac{\sum_{i=1}^{N_p} (G_{ij}/G_{i7})}{N_p}$$

because it is desirable to treat all the shape control points with equal importance. The relative average weighting given in Eq. (3) places an equal importance to each shape control point.

With this PF coil weighting factor, a standard PID feedback control system can be designed by the feedback law,

$$G' \cdot \vec{\Delta} I = g_p \vec{\Delta}\psi + g_I \int \vec{\Delta}\psi \, dt$$

$$\vec{\Delta} V = g_p^v \vec{\Delta} I,$$

where $G'$ is the generalized Green function matrix with PF coil weighting factors,

$$\mathbf{G}' = \begin{bmatrix} G_{11} & G_{12} & G_{13} & G_{14} & G_{15} & G_{16} & G_{17} \\ G_{21} & G_{22} & G_{23} & G_{24} & G_{25} & G_{26} & G_{27} \\ G_{31} & G_{32} & G_{33} & G_{34} & G_{35} & G_{36} & G_{37} \\ G_{41} & G_{42} & G_{43} & G_{44} & G_{45} & G_{46} & G_{47} \\ \alpha_1 & 0 & 0 & 0 & 0 & 0 & 0 \\ 0 & \alpha_2 & 0 & 0 & 0 & 0 & 0 \\ 0 & 0 & \alpha_3 & 0 & 0 & 0 & 0 \\ 0 & 0 & 0 & \alpha_4 & 0 & 0 & 0 \\ 0 & 0 & 0 & 0 & \alpha_5 & 0 & 0 \\ 0 & 0 & 0 & 0 & 0 & \alpha_6 & 0 \\ 0 & 0 & 0 & 0 & 0 & 0 & \alpha_7 \end{bmatrix}$$

$\vec{\Delta}I(\vec{\Delta}V)$ is the feedback current (voltage) vector,

$$\vec{\Delta}I = \begin{bmatrix} \Delta I_1 \\ \Delta I_2 \\ \Delta I_3 \\ \Delta I_4 \\ \Delta I_5 \\ \Delta I_6 \\ \Delta I_7 \end{bmatrix}, \qquad \vec{\Delta}V = \begin{bmatrix} \Delta V_1 \\ \Delta V_2 \\ \Delta V_3 \\ \Delta V_4 \\ \Delta V_5 \\ \Delta V_6 \\ \Delta V_7 \end{bmatrix},$$

$\vec{\Delta}\psi$ is the flux error vector,

$$\vec{\Delta}\psi = \begin{bmatrix} \Delta\psi_1 \\ \Delta\psi_2 \\ \Delta\psi_3 \\ \Delta\psi_4 \\ 0 \\ 0 \\ 0 \\ 0 \\ 0 \\ 0 \\ 0 \end{bmatrix},$$

where $\Delta\psi_i$ denotes the flux difference between a flux at the desired plasma shape control point and a X-point flux, $g_p$ ($g_I$) is a proportional (integral) gain and $g_p^v$ is a proportional gain in the voltage level. In the next subsection, the results of shape control simulations using different coil weighting factors, namely, the constant weighting with constant $\alpha_j$ and the Green function weighting (GW) with $\alpha_j = \bar{f}_j$, will be compared.

### 3.2. Shape control simulations

In this subsection, we apply the shape control system described in the previous subsection to a shape control simulation. As a model disturbance, we choose a high $\beta$ plasma [$\beta_N = 5.0$, $l_i(3) = 0.8$] with the nominal KSTAR plasma parameters, given in Table 1, undergoing 20% permanent $\beta$ drop at $t = 10$ ms. The fast radial position control system utilizing IRC, and the shape control system using seven PF coils are turned on at $t = 10$ ms. Two separate control simulations using different coil weighting method (constant $\alpha_j$ and $\alpha_j = \bar{f}_j$) are performed and compared. At the moment, we do not employ the shape identification algorithm to calculate flux errors because our main interest here is the comparison of the shape control performance between the two different coil weighting methods. The same values of $g_p$, $g_I$ and $g_p^v$ are used throughout the simulations. The constant coil weighting factor $\alpha$ is adjusted to be, $\alpha = \bar{f}_j / N_p$ in order that the comparison between the two coil weighting methods is more accurate.

Figs. 12 and 13 show the errors in the four shape control points during simulations. The performance of a shape control system could be measured by such quantities as the maximum deviations from desired values and the saturated levels of shape errors. In this sense, it can be deduced from Fig. 12 that the constant and the GW coil weighting methods give rise to quite a similar shape control performance, although the feedback currents in PF coils are different.

Figs. 14 and 15 represent the time histories of the currents and voltages of PF4 and PF7, respectively, during the simulations. For simplicity, we present only the results for PF4 and PF7 as typical examples of PF coil behavior during a shape control action. The voltage limits of all the PF coils are fixed to be 30 V. Figs. 14a and 15a clearly show the difference between the two different coil weighting methods. In case of the constant coil weighting method, the feedback current in PF4 is minimized because of small impact of PF4 on shape control points while the burden on PF7 is large, resulting in the long duration of the voltage saturation in PF7. Using the GW coil weighting method, however, the role of PF4 is strengthened and the burden on PF6 and PF7 is ameliorated, resulting in the reduction of the duration of the voltage saturation in PF6 and PF7. The shortened duration of the voltage saturation in PF6 and PF7 produce a benefit of the decrease of a total feedback current and power while yields a similar shape control performance with the constant coil weighting method, as discussed shortly.

Fig. 16 represents the comparison of instantaneous total absolute power, $|P_{abs}| = \Sigma_{i=1}^{N_p} |V_i I_i|$, for two coil weighting methods during simulations. The peak absolute power for constant weighting

is 113 MW while that of GW coil weighting is 91 MW. It is manifested from Fig. 16 that the GW coil weighting method can significantly reduce the required maximum feedback power. The maximum power difference is about 60 MW at $t \sim 0.1$ s. Fig. 17 shows the total feedback current required for a shape control action during simulations. The feedback current reaches its maximum value at $t \sim 60$ ms for the constant coil weighting case. The maximum feedback current for the GW coil weighting case is reduced to about 38% compared with that of the constant coil weighting due to the mitigation of burden on PF6 and PF7. The saturated values of the total feedback current for both the coil weighting cases are approximately the same. We can conclude that the GW coil weighting strategy is beneficial because it controls shape errors with a reduced total feedback current and power within voltage limits of power supplies.

Until now, we have assumed that flux errors are given exactly by TSC. In real experiments, however, the flux errors should be calculated by adopting a real-time shape identification method. In order to assess the performance of a shape control system in real experiments, we perform shape control simulations using calculated flux errors. The same method given in Section 2 is utilized to calculate flux errors. The calculation of

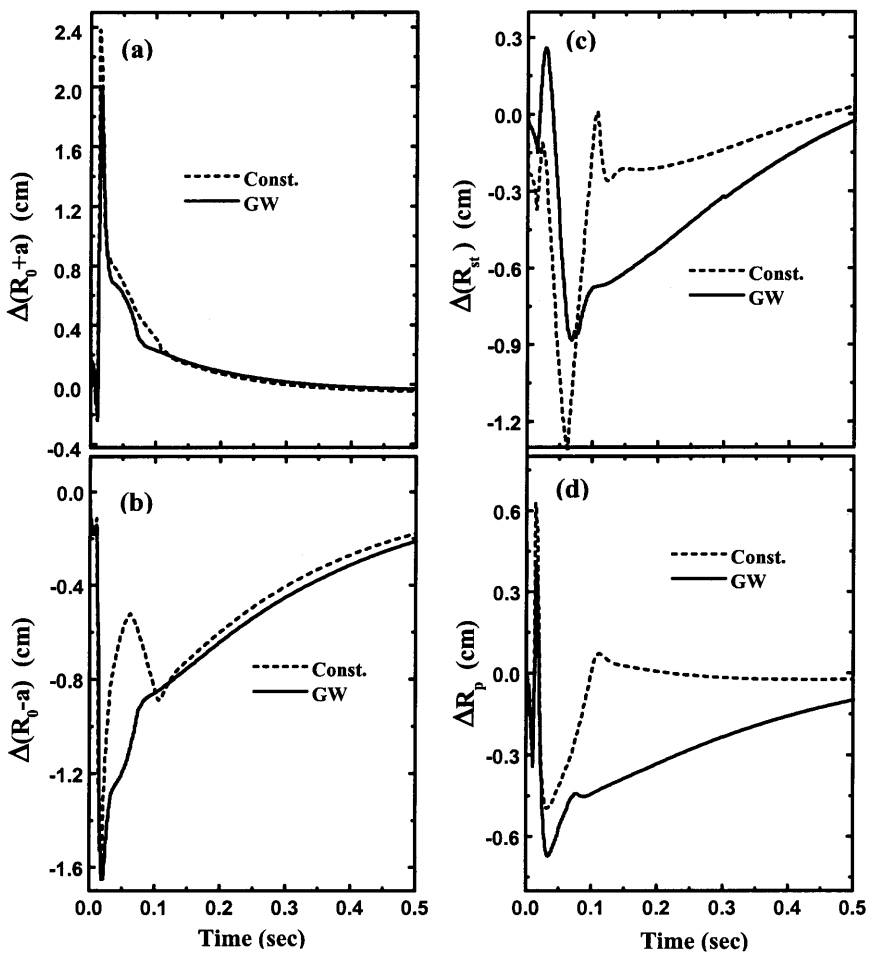


Fig. 12. Errors in (a) $R_0 + a$; (b) $R_0 - a$; (c) passive plate point; and (d) outer strike point during a simulation with a 20% permanent drop in the plasma stored energy. We assume that the flux errors are given exactly by TSC.

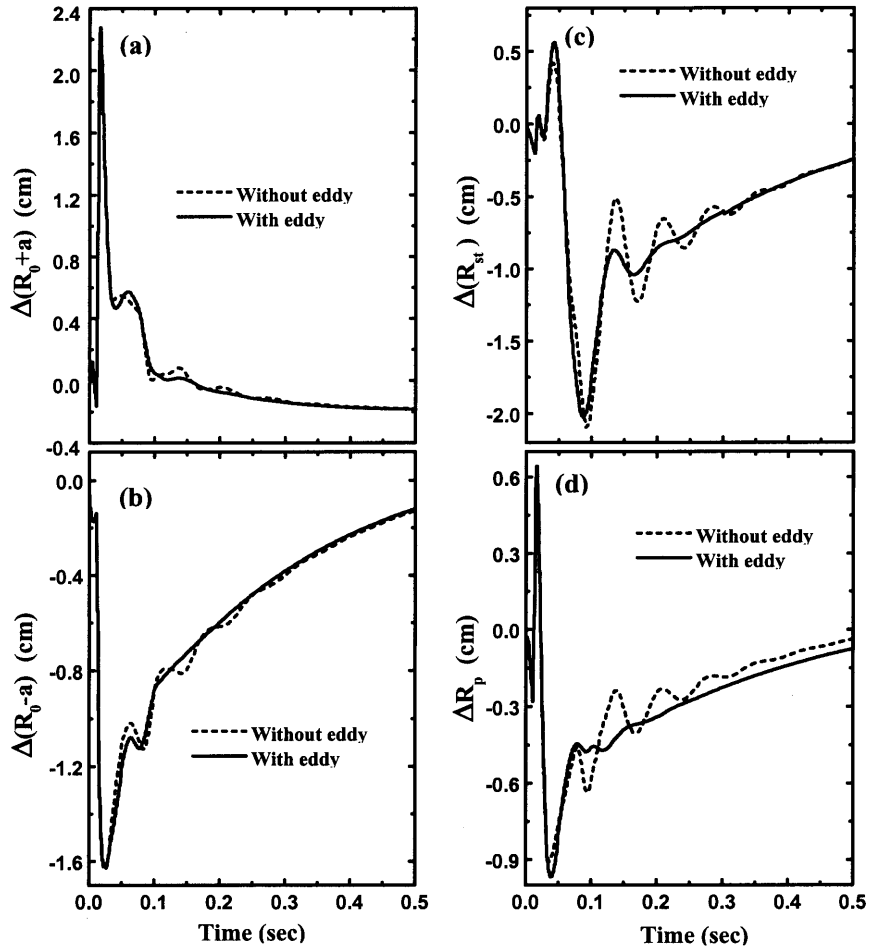


Fig. 13. Errors in (a) $R_0 + a$; (b) $R_0 - a$; (c) passive plate point; and (d) outer strike point during a simulation with a 20% permanent drop in the plasma stored energy. The flux errors are calculated by employing the current element method. Here, the magnetic diagnostic set #1 has been used.

flux errors and feedback currents are realized every 5 ms. Figs. 13, 14b, 15b and 17b represent the time histories of shape errors, coil currents and voltages of PF4 and PF7, and total feedback currents, respectively. In these simulations, the GW coil weighting factor is used and other conditions are exactly the same as those of the previous simulations using exact flux errors.

In order to investigate the consequences of neglecting the eddy currents, two separate simulations are performed and compared — with and without knowing the eddy currents in passive plates. As shown in Figs. 13, 14b, 15b and 17b, the ignorance of eddy currents results in oscillations of shape errors, and coil currents and voltages in the early phase of a shape control action due to the inaccuracy of shape error estimation in early time, as discussed in Section 2.3.2. The oscillation levels of the shape errors and actuator signals are tolerable in this case due to the small up–down symmetric total eddy current (see Section 2.3.2). However, it should be pointed out that a failure of a shape control action would be possible if the total eddy current exceeds some threshold value. Thus, we must take the eddy currents into account in the calculation of flux

errors either by measuring or reconstructing the eddy currents. In KSTAR, the direct measurement of eddy currents in passive plates is under consideration as one of the baseline magnetic measurements. The initial oscillations are greatly reduced by incorporating the eddy currents, as can be seen in Figs. 13, 14b, 15b and 17b. The final saturated values of the shape errors, coil currents, and the voltages are similar to those of the previous simulations using exact flux errors, which indicates the high level of accuracy of the shape identification method.

## 4. Summary and conclusions

In the present work, a comprehensive simulation study for designing a model shape controller has been described and applied to the design of a shape controller for the proposed KSTAR tokamak. It includes the determination of magnetic diagnostic sets, static and dynamic shape identification, and shape control. The basic simulation tool adopted in the study is TSC. The interaction between the plasma and surrounding conducting structures (passive and active coils) can be accurately modeled by using the dynamic capability of TSC.

It has been shown that the total number of magnetic measurements can be effectively reduced by evaluating magnetic fluxes and fields along a measurement contour. The proposed reduced sets satisfy design requirements both in static and dynamic cases. In fact, they showed similar shape identification accuracy compared with that of originally proposed sets. The optimization

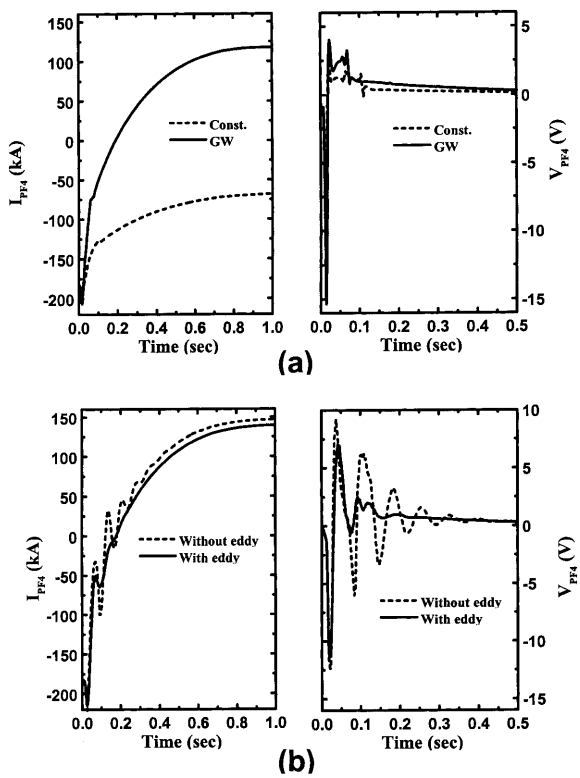


Fig. 14. Time histories of the current and voltage of PF4 during the shape control simulation using (a) the exact flux errors given by TSC, and (b) the calculated flux errors.

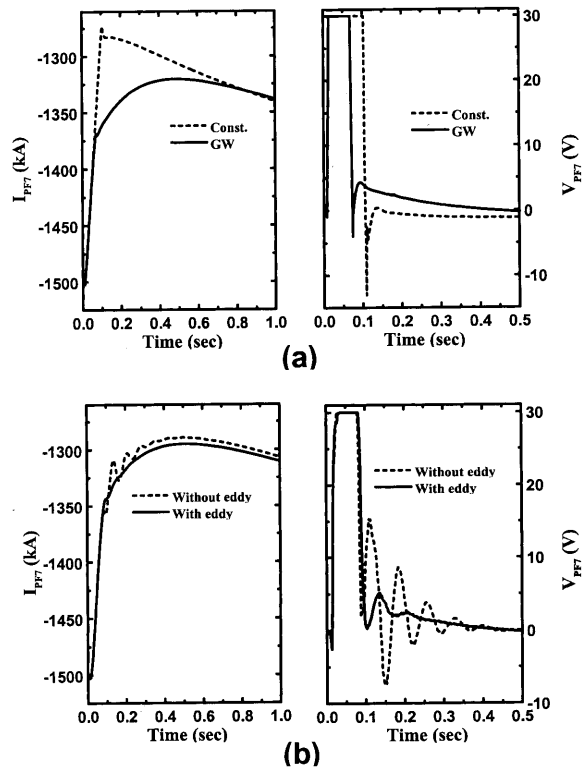


Fig. 15. Time histories of the current and voltage of PF7 during the shape control simulation using (a) the exact flux errors given by TSC, and (b) the calculated flux errors. Note that the measurement of eddy currents reduces initial oscillations of the currents and voltages of PF coils.

method proposed in this paper would be useful in determining an optimum magnetic diagnostic set for the next generation tokamaks, such as ITER.

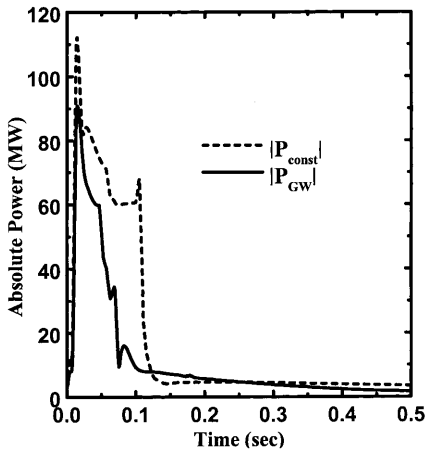


Fig. 16. Total absolute feedback power for the constant and GW coil weighting schemes during the shape control simulation in Fig. 12. Note that the GW coil weighting can greatly reduce the total feedback power required for a shape control action.

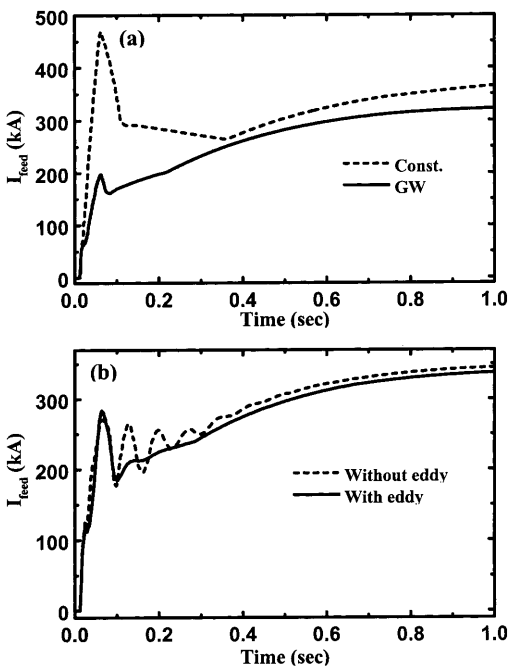


Fig. 17. Total feedback currents required for a shape control action using (a) the exact flux errors given by TSC, and (b) the calculated flux errors.

The finite current density element method, which is currently used in TCV, has been employed in the present study. It has been shown that the method accurately identified the plasma shapes both in static simulations with a maximum 2% random measurement error and in dynamic simulations with and without knowing eddy currents. A similar study was also carried out by using the filament method [3], which uses some filaments located along a contour inside a plasma to represent a plasma current. The major advantage of the finite current element method is that the location of current density nodes does not have to be changed in time, as indicated by original authors [4]. The overall accuracy of both the methods was quite similar although it depended on the number and the location of the current filaments (and/or current density nodes).

The effect of eddy currents on shape identification has been investigated from dynamic simulations. The errors in shape identification are transient and different from point to point due to the difference of $L/R$ times of nearby passive conducting structures. A total up–down symmetric eddy current up to 20 kA does not greatly affect the shape identification accuracy. However, it has also been shown that the errors in shape identification due to the neglected eddy currents can lead to oscillation of actuator signals (PF coil currents and voltages) when the shape identification process is combined into a shape controller. The up–down asymmetric eddy currents caused by a vertical movement of a plasma can be cancelled out by averaging the flux and field measurements hence, does not affect the accuracy of a time averaged shape identification.

It has been shown that it is important to incorporate appropriate weighting factors of PF coils to maximize the shape control capability while minimizing a total feedback power, in the presence of the practical voltage limits in power supplies. A simple method of evaluation of a PF coil weighting factor based on the Green function between PF coils and shape control points has been proposed and tested. The proposed PF coil weighting method has been applied to the simulation of a response to drop in the plasma stored

energy. It has been shown that the total feedback current and power required for a shape control action can be greatly reduced compared with that of a standard isoflux control scheme using a constant coil weighting factor.

The shape control simulations using calculated flux errors have been performed to investigate the performance of a proposed shape controller in real experimental situations. It has been pointed out that neglecting the eddy currents can result in the initial oscillation of actuator signals, which should be avoided for a successful and stable shape control action. Thus, the incorporation of eddy currents in passive conducting structures is important for the stable operation of a shape control system in tokamaks. In the present work, we assumed that the measurement of passive plate eddy currents is available. If it is not the case, the eddy currents should be reconstructed by treating them as nodes of the unknown current matrix.

Finally, we remark that the methods and results of the present work will be useful for currently operating tokamaks as well as the design of the next generation tokamaks.

## Acknowledgements

This work was supported by the Korea Ministry of Science and Technology under KSTAR Project Contract.

## References

[1] G.S. Lee, J. Kim, S.M. Hwang, C.S. Chang, H.Y. Chang, M.H. Cho, et al., The design of KSTAR tokamak, Fusion Eng. Des. 46 (1999) 405–411.
[2] H. Jhang, C. KesselL, N. Pomphrey, S.C. Jardin, G.S. Lee, C.S. Chang, Design calculations for fast plasma position control in Korea superconducting tokamak advanced research, Fusion Eng. Des. 45 (1999) 101–115.
[3] D.W. Swain, G.H. Neilson, An efficient technique for magnetic analysis of non-circular high-beta tokamak equilibria, Nucl. Fusion 22 (1982) 1015.
[4] F. Hofman, G. Tonetti, Fast identification of plasma boundary and X-points in elongated tokamaks, Nucl. Fusion 28 (1988) 519–522.
[5] D.K. Lee, Y.-K.M. Peng, An approach to rapid plasma shape diagnostics in tokamaks, J. Plasma Phys. 25 (1981) 161–173.
[6] K. Kurihara, Improvement of tokamak plasma shape identification with a Legendre–Fourier expansion of the vacuum poloidal flux function, Fusion Technol. 22 (1992) 334–349.
[7] D.P. O'Brien, J.J. Ellis, J. Lingertat, Local expansion method for fast plasma boundary identification in JET, Nucl. Fusion 33 (1993) 467–474.
[8] M. Matsukawa, N. Hosogane, H. Ninomiya, Application of regression analysis to deriving measurement formulas for feedback control of plasma shape in JT-60U, Plasma Phys. Control. Fusion 34 (1992) 907–921.
[9] B.J. Braams, W. Jilge, K. Lackner, Fast determination of plasma parameters through function parametrization, Nucl. Fusion 26 (1986) 699–708.
[10] J.B. Lister, H. Schnurrenberger, Fast non-linear extraction of plasma equilibrium parameters using a neural network mapping, Nucl. Fusion 31 (1991) 1291–1300.
[11] J.R. Ferron, M.L. Walker, L.L. Lao, H.E. St. John, D.A. Humphreys, J.A. Leuer, Real time equilibrium reconstruction for tokamak discharge control, Nucl. Fusion 38 (1998) 1055–1066.
[12] J.B. Lister, F. Hofmann, J. Moret, F. Buhlmann, M.J. Dutch, D. Fasel, et al., The control of tokamak configuration variable plasmas, Fusion Technol. 32 (1997) 321–373.
[13] F. Hofmann, S.C. Jardin, Plasma shape and position control in highly elongated tokamaks, Nucl. Fusion 30 (1990) 2013.
[14] S.C. Jardin, N. Pomphrey, J. Delucia, Dynamic modeling of transport and positional control of tokamaks, J. Comput. Phys. 66 (1986) 481–507.
[15] R. Albanese, G. Ambrosino, E. Coccorese, F.C. Morabito, A. Pironti, G. Rubinacci, et al., Plasma current, shape and position control in ITER, Fusion Technol. 30 (1996) 167–183.
[16] A. Portone, R. Albanese, Y.V. Gribov, M. Huguet, D.H. Humphreys, C.E. Kessel, et al., Dynamic control of plasma position and shape in ITER, Fusion Technol. 32 (1997) 374–389.
[17] I.H. Hutchinson, S.F. Horne, G. Tinios, S.M. Wolfe, R.S. Granetz, Plasma shape control: a general approach and its application to Alcator C-Mod, Fusion Technol. 30 (1996) 137–149.